Eco-friendly synthesis of SiO2 nanoparticles confined in hard carbon: A promising material with unexpected mechanism for Li-ion batteries

Cristina Nita, Julien Fullenwarth, Laure Monconduit, Jean-Marc Le Meins, Philippe Fioux, Julien Parmentier, Camelia Matei Ghimbeu

Eco-friendly synthesis of SiO_2 nanoparticles confined in hard carbon: A promising material with unexpected mechanism for Li-ion batteries

Cristina Nita [a, b], Julien Fullenwarth [c, d], Laure Monconduit [c, d], Jean-Marc Le Meins [a], Philippe Fioux [a], Julien Parmentier [a], Camélia Matei Ghimbeu [a, d, *]

[a] Université de Strasbourg, Université de Haute-Alsace, Institut de Science des Matériaux de Mulhouse (IS2M), UMR 7361 CNRS-UHA, 15 rue Jean Starcky, BP 2488, 68057, Mulhouse Cedex, France
[b] Center for Advanced Laser Technologies (CETAL), National Institute for Lasers, Plasma and Radiation Physics, Atomistilor 409 bis, RO-77125, Magurele, Romania
[c] ICG/AIME (UMR 5253 CNRS), Université Montpellier II CC 15-02, Place E. Bataillon, 34095, Montpellier Cedex, France
[d] Réseau sur le Stockage Electrochimique de l'Energie (RS2E), CNRS FR3459, 33 Rue Saint Leu, 80039, Amiens Cedex, France

A B S T R A C T

A fast, simple and environmentally friendly one-pot route to obtain carbon/SiO_2 hybrid materials is reported in this work. This consists in simple mixture of carbon and silica precursors, followed by thermal annealing at different temperatures. An interpenetrating hybrid network composed of hard carbon and amorphous SiO_2 nanoparticles (2–5 nm) homogeneously distributed was achieved. Increasing the annealing temperature from 600 °C up to 1200 °C, the material porosity and oxygen functional groups are gradually removed, while the amorphous nature of SiO_2 is conserved. This allows to diminish the irreversible capacity during the first charge-discharge cycle and to increase the reversible capacity. An excellent cycling capability, with a reversible capacity up to 535 mA hg^{-1} at C/5 constant current rate was obtained for C/SiO_2 materials used as anodes for Li-ion batteries. An atypical increase of the capacity during the first 50 cycles followed by a stable plateau up to 250 cycles was observed and related to electrolyte wettability limitation through the materials, particularly for those annealed at high temperatures which are more hydrophobic, less porous and the SiO_2 nanoparticles less accessible. The SiO_2 lithiation mechanism was evaluated by XRD, TEM and XPS post-mortem analyses and revealed the formation of reversible lithium silicate phases.

1. Introduction

During the last years a lot of research has been focused on batteries studies, these being one of the most important key for the technology development. Lithium-ion batteries are widely used throughout the world for portable electronic devices and mobile phones and show a great potential for more energy demanding applications like electric vehicles [1]. Currently, graphite is the anode material used in commercial Li-ion batteries mainly owing to its low and flat voltage plateau at about 0.1–0.2 V during discharge, great stability and capacity retention combined with low price [2,3]. However, the theoretical gravimetric capacity of graphite is low (372 mA h/g) for large-scale applications like electric vehicles due to the limited Li insertion (one Li atom for six carbon atoms). Consequently, during the last years there is an increased demand to develop novel and improved anode materials exhibiting a high capacity.

In this purpose, carbon/Si-based materials have been intensively studied as anodes for lithium ion batteries [4–7], especially because of the high abundance of Si in the earth crust [8,9] and its high theoretical capacity of 3579 $mAhg^{-1}$ at room temperature [10]. The large capacity of silicon is associated to the ability of silicon atoms to bond with up to approximately four lithium ions (stoichiometry of $Li_{15}Si_4$) [11]. However, the insertion of Li triggers a high volume expansion/contraction (more than 300%) due to the formation of $Li_{15}Si_4$ alloy compounds [11], which induce stress and strain in the silicon particles, causing some internal cracks and even breakage (pulverization). The Solid Electrolyte Interface (SEI) layer formed as a result of the reactivity of electrolyte on Si become unstable

leading to poor cycling performances [12]. Moreover, the contraction of the volume during the delithiation leads to the agglomeration and electrical isolation of the Si particles from the conductive carbon network, which causes also a drastic decrease of the capacity during cycling. Many studies were performed in order to find the appropriate conditions to limit the agglomeration of the particles and, implicitly, the capacity loss, these being focused on the control of the particle's size and their coating with carbon layers [13]. Because of the difficulty or long procedures to synthesize metallic Si particles or C/Si composites [13–18], lately researches have been redirected towards SiO_2 materials as anode for Li-ion batteries. The lithiation mechanism widely used in the literature is based on the reduction reaction of SiO_2 with the formation of Si and Li_2O, and subsequent insertion of Li in Si with the formation of Li_xSi alloy [5]. A high specific capacity is expected with SiO_2 based on this mechanism, however, practically these values are not achieved due to large volume expansion, formation of irreversible lithium oxide and lithium silicate during cycling and low electronic conductivity. Therefore, there is a great challenge to design nanosize SiO_2 particles/carbon composites gathering the advantages of both materials, i.e. small particle size to reduce lithium diffusion path length and the carbon matrix to provide the electronic pathways and to limit the volume expansion and structural strain during charge/discharge cycles. Recently, Xia et al. [19] prepared SiO_2 nanocrystals embedded in a carbon matrix through hydrothermal approach followed by carbonization in N_2 atmosphere. The electrochemical tests were performed at 100 mAg^{-1} and a reversible capacity of 888 $mAhg^{-1}$ was retained for 100 cycles. In the same time, a high irreversible capacity was observed after the first cycle, the columbic efficiency being only approximately 59%. Hao et al. [20] reported also amorphous silica embedded in mesoporous carbon support, the preparation involving the co-assembly of a triblock polymer template (Pluronic F-127), a silica source (TEOS, tetraethyl orthosilicate) and a carbon source, resol, obtained by polymerization of toxic phenol and formaldehyde precursors, followed by pyrolysis at 900 °C in N_2 atmosphere and ball milling. The reported reversible capacity was ranged between 300 and 670 $mAhg^{-1}$ for different materials, but at low current rate (50 mAg^{-1}) and for a limited number of cycles (12 cycles). Liu et al. [21] synthesized SiO_2 shells covered by carbon through hydrolysis of TEOS, followed by the addition of sucrose dissolved in an acidic water/ethanol solution, ultrasonication and heat treatment in Ar at 800 °C. The reversible capacity continuously increased during the 160 cycles studied, reaching a maximum of 649 $mAhg^{-1}$ for an optimum SiO_2/carbon ratio adjusted by sucrose variation. Preparation of carbon-coated porous silica particles was also reported as anode for Li-ion batteries [22]. The SiO_2 particles preparation involved a silica source (TEOS), several polymeric templates, centrifugation, hexane washing and calcinations. As-prepared SiO_2 macroparticles were covered with carbon by using an aqueous solution of sucrose containing boric acid or not, followed by carbonization at 900 °C under Ar. The reversible capacity presents, like in the previous case, a gradually increase from 195 after the first cycle up to 503 $mAhg^{-1}$ after 103 cycles, at a 200 mAg^{-1}. However, no explanation has been provided for this behavior.

Therefore, different synthesis routes allow to obtain C/SiO_2 materials having various microstructures, morphologies and compositions and therefore different electrochemical performances. It is noteworthy that in most of the cases, the SiO_2 materials were prepared using complex procedures involving several steps, toxic precursors and sacrificial templates. In addition, the materials were cycled only for a limited number of cycles (about 100 cycles) and atypical evolution of the capacity during cycling was observed and the involved storage mechanism not yet addressed.

In this study, we report a very simple, fast and scalable eco-friendly route of preparation for hard carbon/SiO_2 materials which can be successfully used as anode for Li-ion batteries. The one-pot route proposed herein involves a simple mixing between the green carbon and SiO_2 precursors in a water-based solution at room temperature in the absence of any template or strong acids. The influence of heat-treatment temperature was investigated, and the C/SiO_2 treated at higher temperatures exhibit the best performances (~535 $mAhg^{-1}$) and a stable capacity between 50 and 250 cycles. The electrochemical characteristics (reversible and irreversible capacity as well as cycle stability) are discussed in term of material porosity, surface chemistry and SiO_2 particle size distribution. The involved species formed upon lithiation were assessed by XRD and XPS post-mortem analyses suggesting a lithiation *via* reversible formation of lithium silicate compounds.

2. Materials and methods

2.1. Material synthesis

Triblock copolymer Pluronic F-127, phloroglucinol (1,3,5-benzentriol, $C_6H_6O_3$), glyoxylic acid ($HCOCO_2H{\cdot}H_2O$), tetraethyl orthosilicate (>99%, $C_8H_{20}O_4Si$, TEOS), ethanol (C_2H_6O) were purchased from Sigma-Aldrich and used without purification.

The one-pot route developed for the material preparation is illustrated in Fig. 1. The protocol consists in a simple mixing between the carbon and SiO_2 precursors in a water/ethanol solution at room temperature, followed by the evaporation of the solvent which leads to the formation of the phenolic resin – silica gel composite and, finally, to the C/SiO_2 after a heat treatment in Ar atmosphere.

Different carbon/SiO_2 materials were prepared in order to study the influence of the thermal treatment temperature on the physico-chemical characteristics and electrochemical performance. The synthesis is prepared in a teflon jar seated in an oil bath, at 26 °C. The carbon precursors, i.e., phloroglucinol (0.82 g) and glyoxylic acid (0.8 g) were dissolved in 40 ml ethanol-water solution (1:3, volume ratio), followed by the addition of tetraethyl orthosilicate (TEOS, 1.3 ml). The obtained solution is stirred until complete evaporation of the solvent. At the beginning, the solution is colorless and transparent (Fig. S1a, SI), but when the solvent is totally evaporated, a polymeric gel with a rusty brown color is obtained, color related to polymerization reactions between the phloroglucinol and glyoxylic acid (Fig. S1b, SI). Once the material was dried at room temperature, thermal annealing under Ar (10 L/h) with a heating rate of 2 °C/min was performed at four different temperatures: 600, 750, 900 and 1200 °C (C/SiO_2@T, where T denotes the temperature used) (Fig. S1c, SI).

2.2. Physico-chemical characterization

The crystalline structure of the materials was characterized by X-ray powder diffraction (XRD) technique, by using a powder diffractometer D8 ADVANCE A25 from Bruker in Bragg-Brentano reflexion geometry θ – θ. This diffractometer is equipped with the Lynx Eye XE-T high resolution energy dispersive 1-D detector (Cu $K\alpha_{1,2}$) allowing ultra-fast X-ray diffraction measurements. The Raman analyses were performed at room temperature in a back-scattering geometry using a LabRAM BX40 (Horiba Jobin-Yvon) microspectrometer equipped with a He-Ne excitation source (wavelength 532 nm). X-ray photoelectron spectroscopy (XPS) was performed with a VG SCIENTA SES-2002 spectrometer equipped with a concentric hemispherical analyzer. The incident radiation used was generated by a monochromatic Al Kα x-ray source (1486.6eV) operating at 420 W (14 kV; 30 mA). Wide scan spectrum (survey) signal was recorded with a pass energy of 500 eV and for

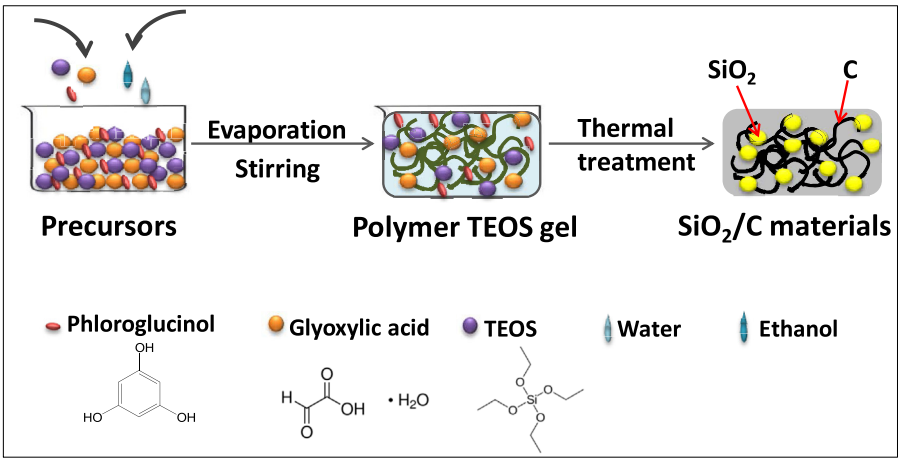

Fig. 1. Schematic representation of the one-pot synthesis protocol developed for C/SiO_2 materials preparation. (A colour version of this figure can be viewed online.)

high resolution spectra (C1s, O1s, Si2p, F1s and Li1s) pass energy was set to 100 eV. Spectra were subjected to a Shirley baseline and peak fitting was made with mixed Gaussian-Lorentzian components with equal full-width-at-half-maximum (FWHM) using CASAXPS version 2.3.18 software. All the binding energies (BE) are referenced to the C1s (graphite-like sp^2 carbon) peak at 284.5 eV and given with a precision of 0.1eV.

The textural properties of the carbon/SiO_2 materials were evaluated using N_2 and CO_2 sorption isotherms. The N_2 adsorption/desorption isotherms were measured with a Micromeritics ASAP 2420 device at 77 K. The samples were out-gassed in vacuum at 250 °C for 12 h before the adsorption analysis. The specific surface area (SSA) was calculated by BET model from the linear plot in the relative pressure range of 0.01—0.05, The micropore volume (V_{micro}) was obtained using the Dubinin-Radushkevich (DR) equation in the relative pressure interval (P/P_0) from 10^{-4} to 10^{-2}. The total pore volume (V_T) was determined from the amount of nitrogen adsorbed at a relative pressure of 0.95. The pore size distribution (PSD) was determined from the adsorption branch of nitrogen isotherms using the 2D-NLDFT heterogeneous surface model for carbon materials implemented in SAIEUS (Micromeritics). The same Micromeritics ASAP 2420 device was used for the CO_2 measurements, but at 273 K, the out-gassing conditions were the same as indicated before.

The material surface morphology/structure was investigated with a JEOL ARM-200F transmission electron microscope working at 200 kV. EDX mapping was obtained with a JED 2300 detector. Contact angle measurements were performed on C@SiO_2 electrodes with a Krüss DSA100 goniometer using water as probe molecule.

2.3. Electrochemical characterization

The electrode was prepared by mixing in a jar the synthesized materials (70 wt.%) with carbon black (10 wt.%) and vapor ground carbon fibers - VGCF-S (10 wt.%) as conductive additives, and carboxymethylcellulose - CMC (10 wt.%) as binder. A quantity of 0.4 ml distillated water was added over the materials and homogeneously mixed by ball-milling for 1 h. The film with a thickness of 100 μm was tape-casted on a copper foil, dried at room temperature for 4 h and at 100 °C under vacuum for other 12 h. Electrodes with a diameter of 14 mm were cut and the corresponding loading of the active mass in the electrode was comprised between 0.9 and 1.9 $mgcm^{-2}$.

The electrochemical performances of carbon/SiO_2 materials as negative electrode for Li-ion batteries were studied in coin cells assembled in an argon filled glove box. The electrolyte used for the coin cell preparation was 1M $LiPF_6$ in a mixture of ethylene carbonate (EC), propylene carbonate (PC) and dimethyl carbonate (DMC) (1:1:3) as solvents. The galvanostatic charge and discharge measurements were carried out at room temperature on Mac pile (Biologic SA and MTI) battery testing system. The electrochemical performances of carbon/SiO_2 materials were evaluated at constant rate, C/5 or in variable regime ranged between C/10 to 3C. The theoretical capacity of Si was considered (3579 $mAhg^{-1}$ corresponding to $Li_{15}Si_4$, the most lithiated alloy form of Si). The capacity is reported per gram of active mass which is considered the mass of carbon/SiO_2 composite.

3. Results and discussions

The XRD patterns of carbon/SiO_2 materials (Fig. 2a), exhibit three broad diffraction peaks, corresponding to the hexagonal graphite structure. The presence of broad peaks indicates a low degree of graphitization in the material. The absence of any other peak indicates the amorphous structure of silica, whose peak ranging between 15 and 30° could be overlapped by the (002) peak of graphite. A slight improvement of the graphitization level with the increase of the annealing temperature was observed by comparing the (100) and (110) peaks, while in the case of the (002) peak, there is no significant difference noticed due to the superposition of the carbon and silica peaks. Raman spectra shows two peaks related to the D (defect) and G (graphite) contributions, characteristic for carbon materials (Fig. 2b). By increasing the temperature, the position of G band slightly decreases from 1598 to 1595 cm^{-1} while for D band a more pronounced decrease is observed, i.e., 1365 to 1346 cm^{-1} from 600 °C to 1200 °C. The same trend is observed for the FWHM (full width at half-maximum) of D band which significantly narrows with the temperature. These results suggest the organization of the material increases with the temperature [23,24]. The I_D/I_G ratio increases with the temperature and can be understood by a growth in size and/or number of crystallites [25]. At low annealing temperature (600 °C), very small crystallites are present in the materials, and do not significantly contribute to Raman spectra. When the annealing temperature increases, the crystallites size and number grow, and thus they contribute more to the Raman spectra resulting in an increase of I_D/I_G ratio [25]. The formation of larger crystalline domains is sustained by the TEM results as presented in Fig. S2,SI. Any pore could be distinguished for C/SiO_2@T materials, the surface being rather

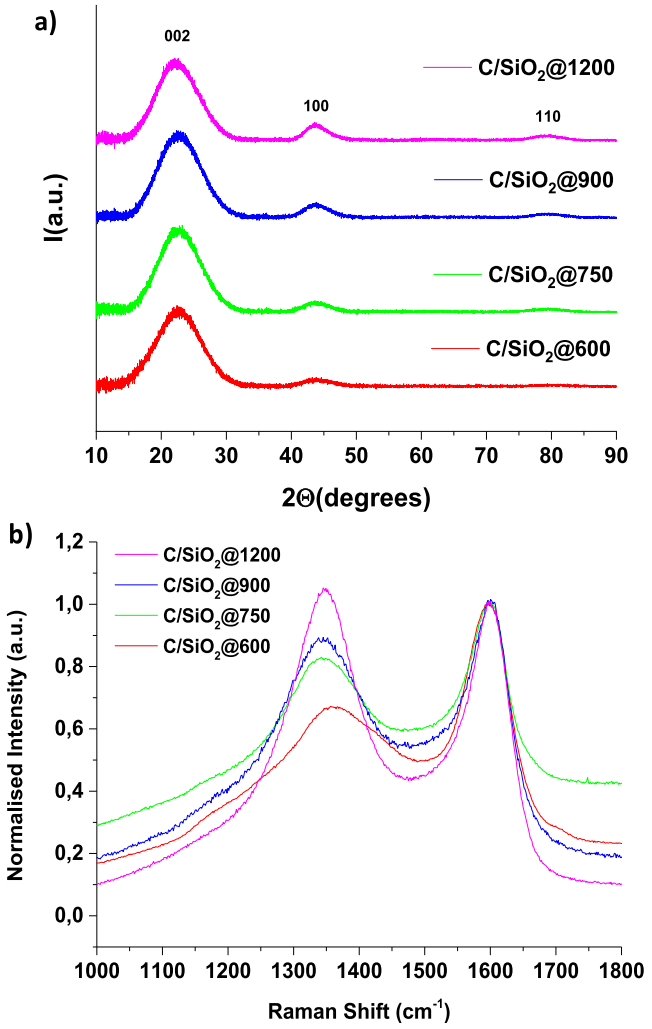

Fig. 2. X-ray diffraction patterns (a) and Raman spectra (b) for carbon/SiO_2 materials obtained using different synthesis conditions. (A colour version of this figure can be viewed online.)

smooth. However, few graphitized domains are observed for high temperature treated materials, C/SiO_2@1200 (Fig. S2 b, SI).

The composition and chemical oxidation state in the surface of the materials (<10 nm thickness) were determined by XPS in the range 0 and 1200 eV. In Fig. 3, the XPS spectra for C/SiO_2@1200 is presented as an example. The survey spectra (Fig. 3a) reveal the presence of C1s, O1s, Si2s and Si2p peaks; all the other materials containing the same components.

The high-resolution C1s XPS spectra (Fig. 3b) shows one intense peak at 284.5 eV, which is assigned to graphite-like sp^2 carbon [26]. The peak was deconvoluted into five components. The first peak situated at 285.0 eV reveals the presence of carbon in α position of carbonyl groups and eventually CH_x carbon species due to atmospheric contamination. The tail of the asymmetric C 1s peak at higher binding energies originates from the presence of carbon atoms bonded to different oxygen-functional groups, i.e., ether/hydroxyl (C–OR), carbonyl (C=O) and carboxyl (O=C–O) placed at 286.2 eV, 287.4 eV and 288.7 eV, respectively [26]. The same analyses were performed for all materials and the obtained spectra indicate the formation of the same groups as described previously (Table 1).

The O1s XPS spectra (Fig. 3c) present one peak which was deconvoluted into five components. The most intense peak is situated at 532.25 eV and corresponds to SiO_2. The peak from 531.3 eV indicates the presence of O=C bonds (Quinone, Phenylcetone); the peak situated at 532.8 eV reveals the O=C-O (carboxyl, anhydride, ester) and that from 534.2 eV to 535.4 eV indicate the chemisorbed and physisorbed H_2O, respectively. The position of Si2p and O1s peaks (103.4 eV and 532.25 eV, respectively), are specific for the SiO_2 formation [21]. Fig. 3d shows the high-resolution Si2p XPS spectra. After the deconvolution, the spectra displays a Si2p doublet, composed of $Si2p^{3/2}$ and $Si2p^{1/2}$ due to spin-orbit coupling, assigned to SiO_2 ($Si2p^{3/2}$–103.4 eV).

The composition analysis for each high-resolution spectrum was performed and the values are gathered in Table 1.

The amount of oxygen groups linked to carbon presents a decreasing trend from 5.21 at. % for C/SiO_2@600 to 3.95 at. % for C/SiO_2@1200, these oxygen groups being removed during the annealing step. The amounts of carbon and Si for the material treated at 600 °C (C/SiO_2@600) are about 71 at.% and 7.25 at.%, respectively. For the materials treated at higher temperature (C/SiO_2@750), the amount of carbon decreases (~64–66 at. %) and that of Si increases (~10 at. %) then remains rather constant between 900 and 1200 °C (C/SiO_2@900 and C/SiO_2@1200). This may be understood by the complete carbonization of the phenolic resin between 600 and 900 °C which lead to the decrease of the carbon amount due to the removal of CO_x and H_2 groups, and consequently to an increase of the SiO_2 amount in the composite.

The O(–Si)/Si ratio for the material treated at 600 °C is about 2.14 (Table 1) while for the materials treated at 750, 900 and 1200 °C this ratio remains rather similar (1.96, 1.92 and 1.95, respectively). These results confirm the formation of SiO_2 in the whole used temperature range.

The composition and thermal/chemical stability of carbon/SiO_2 materials were determined by thermogravimetric analysis (TGA) in air (Fig. S2, SI), which allows the oxidation of carbon and the determination of SiO_2 quantities. The SiO_2 loading was calculated by taking into account the H_2O content for each material, the evaporation of the water taking place before 150 °C (Fig. S3 a, SI). According to Table 1, the SiO_2 loading varies between 28 wt.% and 43 wt.%, as a function of the annealing temperature. The most significant variation of the SiO_2 loading is due to the increase of the temperature from 600 to 750 °C, as a result of the removal of functional groups with the evolution of CO_x gases (x = 1; 2), while for higher temperatures the difference is not significant. The same behavior was observed by XPS (Table 1).

The peak corresponding to the oxidation of the carbon is shifted from 560 °C to 680 °C by increasing the annealing temperature from 600 to 1200 °C (Fig. S3 b, SI). This behavior could be explained on one hand by the decrease of the oxygen content linked to the carbon in the higher temperature annealed samples, therefore a lower reactivity towards O_2. On the other hand, it could be related to the stabilization of the carbon structure by an improvement of the degree of crystallization of the carbon with the temperature (loss of oxygen and better graphitization observed by XPS and XRD), and to the lower surface area of the material (see N_2 adsorption results, Table 2). This lower reactivity of high-temperature treated samples can also be associated with a better passivation effect of SiO_2, acting as a dense layer and hindering the diffusion of oxygen.

The STEM images in dark-field shows the formation of small (2–5 nm) and well distributed SiO_2 particles in the carbon supports no matter the temperature of the thermal treatment (Fig. 4a and b). The Energy Dispersive X-ray (EDX) analysis shows an intimate mixture of C, O and Si atoms, confirming the uniform dispersion of the elements at atomic level (Fig. 4c, d, e). The same homogeneity could be observed also for the materials treated at 750, 900 and 1200 °C. Moreover, for these materials, a slight increase of the

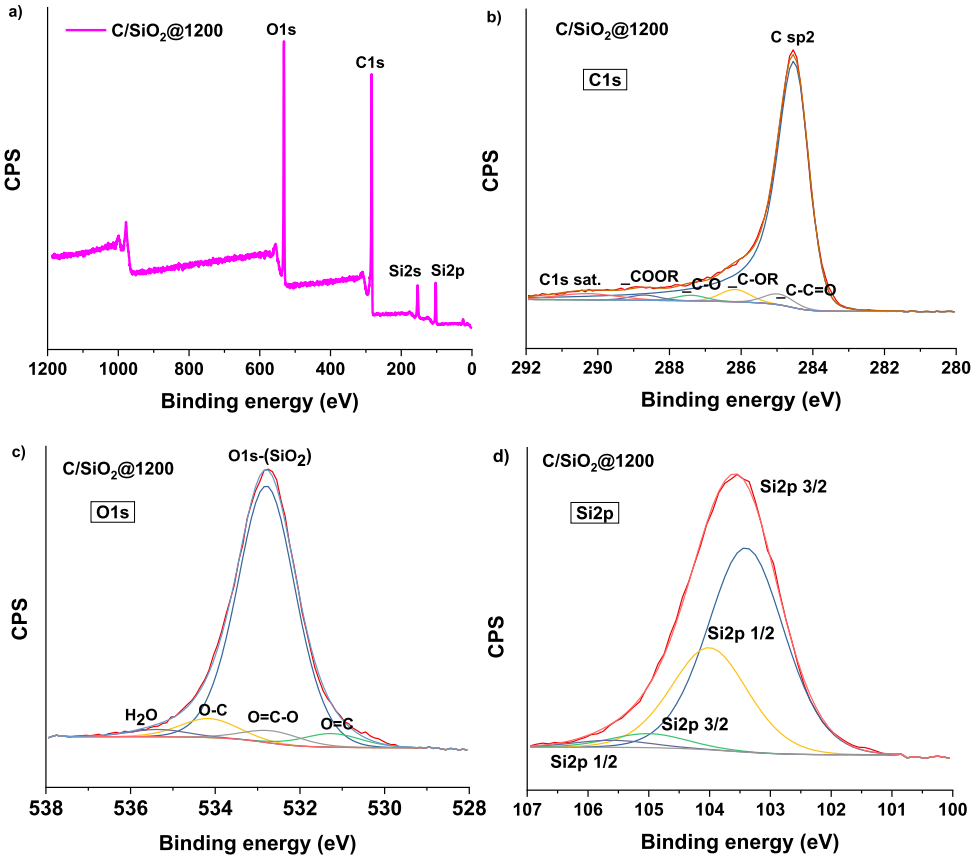

Fig. 3. X-ray photoelectron spectra of C/SiO_2@1200: wide (survey) scan (a), and high resolution deconvoluted spectra of C1s(b), O1s (c) and Si2p (d). (A colour version of this figure can be viewed online.)

Table 1
Chemical composition of the carbon/SiO_2 materials obtained by XPS measurements and SiO_2 quantity determined by TGA analyses..

Material	Chemical composition (at. %)			Repartition of oxygen (at. %)			SiO_2 quantity (wt.%) (by TGA)
	C	Si	O (total)	O (-Si)	O (-C)	O/Si	
C/SiO_2@600	71.03	7.25	20.71	15.5	5.21	2.14	28
C/SiO_2@750	64.13	10.61	25.26	20.77	4.49	1.96	41
C/SiO_2@900	66.75	10.00	23.25	18.69	4.56	1.92	41
C/SiO_2@1200	65.76	10.05	23.51	19.56	3.95	1.95	43

Table 2
Textural properties of carbon/SiO_2 materials determined form N_2 and CO_2 sorption measurements.

Material	N_2 Adsorption			CO_2 Adsorption	
	SSA, $m^2 \cdot g^{-1}$	V_T, $cm^3 \cdot g^{-1}$	V_{micro}, $cm^3 \cdot g^{-1}$	SSA, $m^2 \cdot g^{-1}$	$V_{ultramicro}$, $cm^3 \cdot g^{-1}$
C/SiO_2 @600 °C	403	0.17	0.14	325	0.18
C/SiO_2 @750 °C	339	0.13	0.12	310	0.17
C/SiO_2 @900 °C	120	0.06	0.005	322	0.16
C/SiO_2 @1200 °C	9	0.005	0.004	145	0.09

particle sizes is noticed by increasing the temperature (Fig. S4, SI), which is quite difficult to be quantified because of the high density of SiO_2 particles in the carbon matrix.

The porosity is one of the key parameters that might influence the diffusion of the electrolyte during the cycling tests, the SEI formation and, consequently, the irreversible and reversible capacity. Therefore, the textural properties of the C/SiO_2 materials were evaluated by N_2 and CO_2 sorption isotherms (Fig. 5). The corresponding data are gathered in Table 2.

For all materials, N_2 adsorption/desorption isotherms of type I (Fig. 5a) specific for microporous materials is observed. The decrease of the N_2 up-take in the low relative pressure region with the increase of the heat-treatment temperature indicates a decrease of the micropore volume, a well-known phenomenon related to micropores closure. From Table 2 it can be seen the evolution of the textural properties with the temperature of the thermal treatment. The total pore volume (V_T) decreases with the temperature, from 0.17 $cm^3 g^{-1}$ for 600 °C to 0.005 $cm^3 g^{-1}$ for

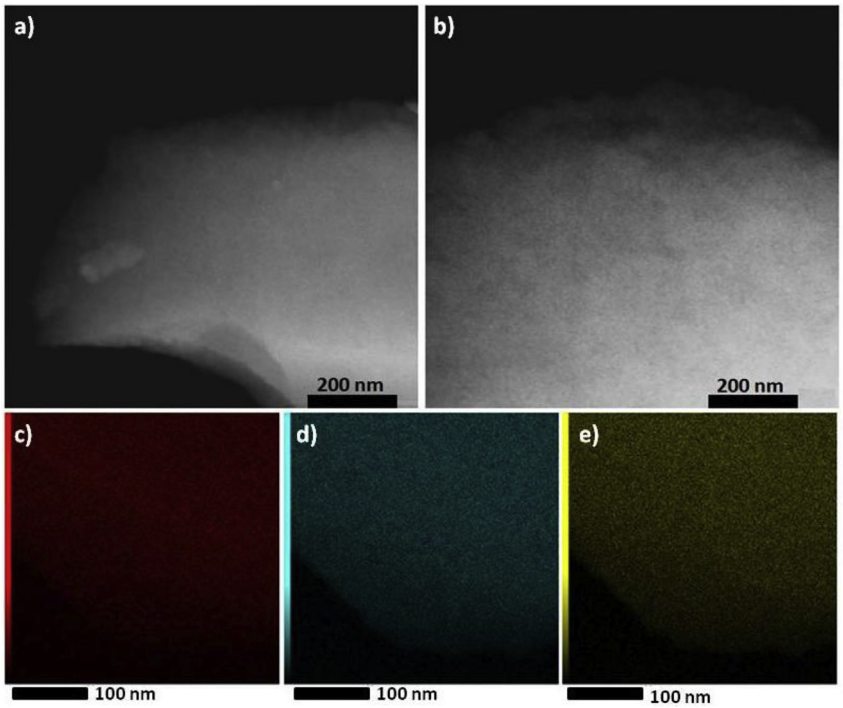

Fig. 4. STEM image for C/SiO_2@600 (a) and C/SiO_2@1200 (b); EDX mapping images for C/SiO_2@600: C (c), O (d), Si (e). (A colour version of this figure can be viewed online.)

1200 °C. The low values of the pore volume for C/SiO_2@1200 suggest rather a non-porous material.

For a better understanding of the micropores evolution, CO_2 adsorption was performed (Fig. 5b) since it allows to better assess the very small pores (<2 nm), the so-called ultra-micropores. For all materials, the determined V_{micro} corresponding to the ultra-micropores is higher than the one determined by N_2. This suggests the co-existence of ultramicropores and micropores in the materials. Interestingly, the evolution of ultramicropores amount with the temperature is rather constant between 600 and 900 °C (0.18–0.16 $cm^3\,g^{-1}$) while that of micropores decreases significantly (0.14–0.005 $cm^3\,g^{-1}$). Therefore, in this temperature range the micropore are closing, while at higher temperature (1200 °C), the ultra-micropores are closing as demonstrated by the significant decrease of the $V_{ultramicro}$ from 0.16 to 0.09 $cm^3\,g^{-1}$. Note that this volume remains still higher than the micropores one (0.004 $cm^3\,g^{-1}$). Therefore, the C/SiO_2@1200, which appeared to be almost non-porous after the N_2 investigation contains plenty of ultra-micropores. The loss of the ultra-microporosity at high temperature may be explained by the reorganization of the graphite layers which results in the microporosity closure or the formation of as called "ink-bottle pores", this phenomena being explained by Falling Card Model [27]. The small opening of these pores does not allow the access of the N_2 atoms, while the CO_2 atoms can penetrate these pores due to their smaller size, and so the micropore volume can be measured by CO_2 adsorption technique.

The pore size distributions (PSD) determined from the adsorption branch of N_2 and CO_2 isotherms (Fig. 5c and d) confirmed the presence of ultramicopores and micropores previously mentioned, located mainly around 0.5 nm and 1 nm. The evolution of the pore volume is the same as discussed before.

All these characterizations highlight that the materials prepared by increasing the temperature present distinct structure, surface chemistry, porosity and size of SiO_2 domains. Such parameters are expected to influence the interactions with the electrolyte and *in-fine* the final performance of the batteries. To predict the interactions of the materials with the electrolyte, wettability measurements were conducted using microdroplets of water settled on the surface of C@SiO_2 electrodes (Fig. 6). As highlighted in Fig. 6a, for low temperature treated samples (600 °C) the contact angle is very small (25.9 °) and the water spontaneously imbibes the material. This behavior is mainly due to the higher porosity and oxygen surface functionalities which favor the adsorption and the hydrophilic interaction of the electrode with the water. When increasing the annealing temperature, the contact angle increases progressively to 30.8°, 39.4° and 44.2°, for 750, 900 and 1200 °C, respectively. This increase in the hydrophobic behavior is in line with the decrease of the porosity and the number of functional groups of the materials.

The influence of the thermal treatment temperature on the electrochemical performances was evaluated *vs.* Li, at a constant current rate of C/5, in the voltage range of 0.01–1.5 V. The capacity evolution for all carbon/SiO_2 materials with the cycle number, are depicted in Fig. 7a. From each material at least two half-cells were prepared in order to check the reproducibility of the results which are presented in Table 3.

The material treated at 600 °C (C/SiO_2@600) presents an irreversible capacity loss during the first cycle of about 78% which decreases with the increase of the synthesis temperature (62% for 1200 °C). This decrease of the capacity loss could be related mainly to the decrease of the SSA [3,28] of the materials and improvement of the carbon structure by increasing the heat temperature (Table 2). As well, the decrease in the number of functional groups (Table 1) may also lead to a decrease in the capacity loss by limiting the decomposition and side reactions of the electrolyte. Moreover, a higher carbonization temperature leads to a higher SiO_2 loading, reducing the irreversibility coming from carbon. A comparison between C/SiO_2@1200 and a pure carbon treated at the same temperature (C@1200) would be interesting in order to evaluate the contribution of carbon. However, in the case of one-pot route, the carbon characteristics are closely related to the reaction medium [29–31], therefore, neither the physico-chemical

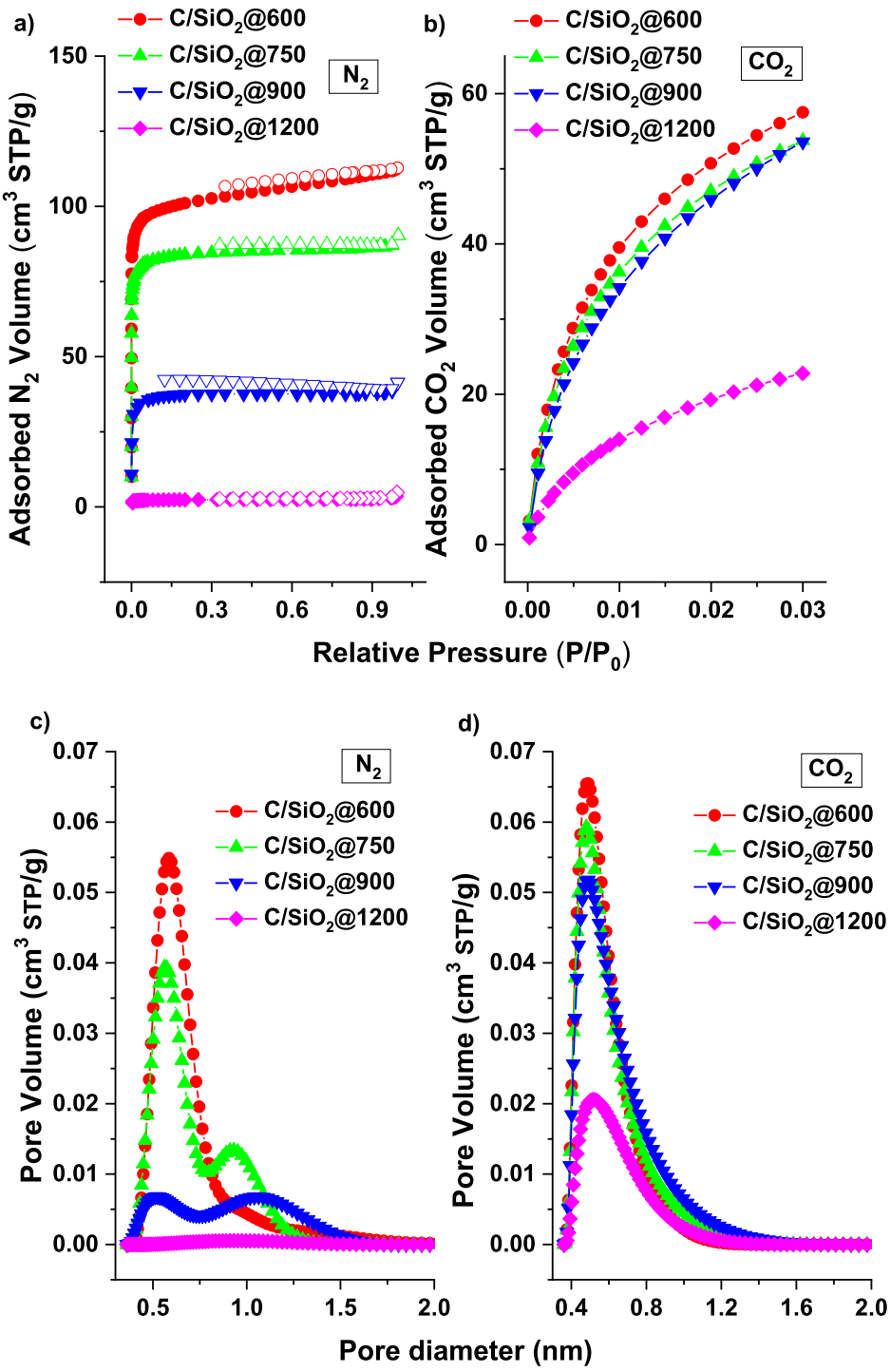

Fig. 5. N_2 adsorption/desorption isotherms (a), CO_2 adsorption isotherms (b), and 2D-NLDFT pore size distribution of carbon/SiO_2 materials obtained from N_2 adsorption (c) and CO_2 adsorption (d). (A colour version of this figure can be viewed online.)

characteristics, nor the electrochemical performances will be the same, and consequently, the comparison will not provide fair information.

A solution to diminish the irreversibility coming from carbon could be the use of a higher SiO_2 loading. Moreover, a positive effect on the irreversible capacity could be obtained by tuning the electrode preparation conditions: i) the additions of some additives to the electrolyte like VC and/or FEC, known for the improvement of stability and reduction of irreversibility; ii) the use of different binders like polyacrylic acid (PAA), alginic acid sodium salt (AA), poly(vinyl alcohol) (PVA) or polyvinylidene difluoride (PVDF), dissolved in water or N-Methylpyrrolidone (NMP) depending on the binder solubility or iii) the use of different combination or ratio between the solvents [11,32,33]. These parameters were not investigated in our study, but their carefully optimization could certainly lead to better electrochemical performances of the materials.

The reversible capacity of the material treated at 600 °C (C/

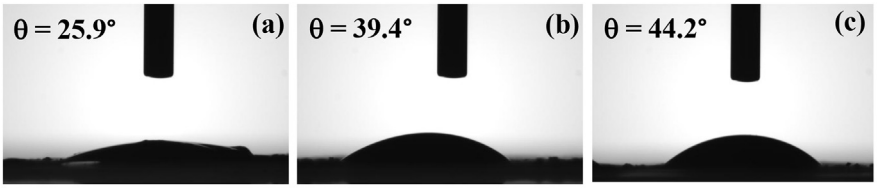

Fig. 6. The contact angles of water distributed on the surface of C@SiO_2 electrodes prepared at different temperatures: 600 °C (a), 900 °C (b) and 1200 °C (c).

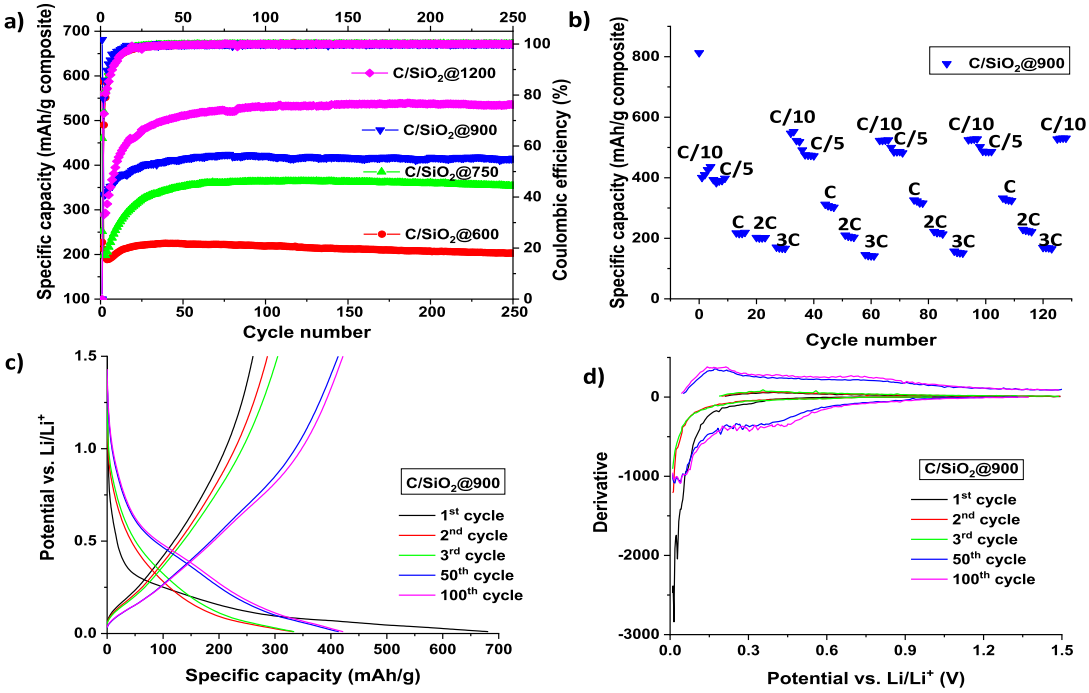

Fig. 7. Discharge capacity and columbic efficiency as a function of cycle number for carbon/SiO_2 materials at a C/5 constant current rate (a) and variable current rate (C/10 to 3C) (b); voltage profiles (c) and differential plots (d) of C/SiO_2@900 material, in the voltage range of 0.01–1.5 V (vs. Li/Li^+).

Table 3
Electrochemical characteristics of carbon/SiO_2 hybrid materials in the voltage range of 0.01–1.5 V (vs. Li/Li^+) and C/5 rate.

Material	First discharge capacity ($mAhg^{-1}$)	First charge capacity ($mAhg^{-1}$)	Irreversible capacity (%)	Capacity 50th cycle ($mAhg^{-1}$)	Capacity 250th cycle ($mAhg^{-1}$)
C/SiO_2@600	588	131	78	224	203
C/SiO_2@750	460	122	73	352	354
C/SiO_2@900	681	261	62	414	415
C/SiO_2@1200	559	210	62	511	535

SiO_2@600) is around 200 mA hg^{-1} which is nicely maintained up to 250 cycles. Surprisingly, after a drastic drop of the capacity after the first cycle, the capacity starts to gradually increase during 50 cycles, then the capacity stabilizes. The reversible capacity after 50 cycles is increasing from 224 mA hg^{-1} to 511 mA hg^{-1} when increasing the material annealing temperature (Table 3), and stabilized after 70 cycles at values between 200 and 535 mA hg^{-1}.

In order to evaluate if this gradual increase of the capacity during the first cycles is due to kinetic limitation, cycling was performed at higher temperature, at 60 °C. In this case, the electrochemical curve does not show anymore the progressive increase of capacity as function of cycle number (Fig. S5, SI), indicating that this atypical gain in capacity could be associated partly to some wettability problems. In the first several cycles, the electrolyte is not wetting efficiently the electrode, limiting in this way, the ion diffusion and, consequently, the material's performances. Little by little, during the cycling, the electrode becomes homogeneously socked in electrolyte, favoring the ions diffusions. The increase of the annealing temperature of the materials leads to the decrease of their porosity and the increase of the hydrophobicity (Fig. 6), therefore the electrolyte needs more time to be well diffused into the electrode, and consequently, the SiO_2 "activation" required higher number of cycles. It is noteworthy that at 60 °C the capacity is stabilized to a value lower than that measured at room temperature. A full systematic study is required to clarify the role played by the temperature on the performance of such systems. On the other hand, the gradually gain in capacity being an atypical behavior for carbon materials, could be more associated to the presence of SiO_2 nanoparticles and, more likely, with their confinement in the carbon structure, which makes them hardly-accessible for the Li ions.

Increasing the annealing temperature from 600 °C to 1200 °C, the carbon becomes more organized and much denser leading even to better confinement of SiO_2 nanoparticles in the carbon network, and therefore more inaccessible to the electrolyte explaining in some extent the higher required charge-discharge cycles to be "activated".

The reversible capacity increase with the annealing temperature coincides with the increase of the SiO_2 content in the composite and decrease of the carbon content (Table 1), which limits the solid electrolyte interphase (SEI) formation due to the decomposition of the electrolyte in presence of carbon. In addition, the increase of the reversible capacity with the annealing temperature could be also related to the small improvement of the graphitization level of the carbon (Fig. 1) and the decrease in porosity. It is worth to note that the evolution of capacity during cycling is particularly stable up to 250 cycles. Moreover, we can mention that the stable cycling for our materials was obtained in absence of any additive in the electrolyte, such as vinylene carbonate (VC) or fluoroethylene carbonate (FEC), which are known for improving the stability of the reversible capacity for Si-based anodes [11,32].

Fig. 7b shows the cycling performances at different current rates for the C/SiO_2 materials treated at 900 °C. The reversible discharge capacities of the composites strongly depend on the C rate but present the same increasing tendency along first cycles identically to cycling obtained at constant current rate. The capacity values decrease to 436, 398, 219, 202 and 167 mA h/g at C/10, C/5, C, 2C and 3C, and when the C rate is increased return to the initial value, the capacity successfully regain 120% from the initial reversible value.

To try to get better insight on the electrochemical lithiation mechanism, the galvanostatic (Fig. 7c) and derivative (Fig. 7d) curves for C/SiO_2 treated at 900 °C are presented. The first discharge profile shows a rapid voltage drop to 0.36 V, attributed to lithium extraction from amorphous carbon, followed by a gradually decrease down to 0.01 V (Fig. 7c). The subsequent two discharge curves are overlapped and present the same trend, indicating similar low electrochemical performances during the first 3 cycles. The derivative curve for the first cycle exhibits only one peak between 0 and 0.15 V characteristic for the reduction of the electrolyte to form the SEI in this carbon rich composite. No other peak is observed in the first 3 cycles, indicating that the reactions in the electrode did not occurred. After 50 and 100 cycles, the shape of the plot is changed, the voltage decreases gradually to 0.01 V and the gain of the reversible capacity which was shown also in Fig. 7a is obvious. After 50 cycles two broad derivative peaks appear in discharge around 0.1 and 0.4 V, and in charge around 0.2 and 0.6 V sign that the reaction between the electrode and the electrolyte has started. In the literature, these positions are assigned to the formation of lithium silicates (Li_xSiO_y)/Li_2O (bellow 0.4 V) and also to Li-Si alloy ($Li_{15}Si_4$, 0.25−0.45 V) [22,34,35] and mainly depend of the characteristics of SiO_2 material.

However, the presence of Si and Li_xSi is difficult to be experimentally assessed especially due to the nanometric size of active material and the insertion of Li in SiO_2 is still not very well understood. To get deeper insight, XRD and STEM analyses were performed on the C/SiO_2@900 post mortem electrodes and compared to their initial state (Fig. 8). While the C/SiO_2@900 initial material is amorphous (Fig. 2a), the XRD patterns performed on the corresponding electrode (Fig. 8a) show the presence of a well-defined peak placed at ~26°, which could be related to the hexagonal phase of graphite (PDF 41−1487). This contribution is due to the graphite additive used in the electrode formulation to improve the material conductivity. After 250 cycles, several other peaks are observed and indexed to lithium carbonate (Li_2CO_3), PDF 87−0728. The presence of Li_2CO_3 is a result of the SEI layer formation as a consequence of electrolyte/solvent decomposition on the material surface. No crystalline phases corresponding to Si-Li have been observed. The Li−Si electrochemical alloying process induce metastable Si-Li phases which are amorphous and therefore not detected by XRD or SAED techniques [36].

STEM analyses were performed on the electrodes C/SiO_2 treated at 900 °C recovered after cycling (Fig. 8b). As it can be seen the carbon and SiO_2 are very well interconnected, some larger particles compared to the initial particles in the pristine electrode are observed, however their size is less than 10 nm. This suggests that the carbon network limits the SiO_2 particle size growth and agglomeration during cycling explaining the stable observed capacity of these materials.

XPS technique was used to get more insights on the formed compounds during the cycling and the possible insertion mechanisms. The C/SiO_2@900 after 250 cycles was analyzed and the survey spectra showed no peaks assigned to SiO_2 and only a very small peak corresponding to sp^2 carbon was observed in the high resolution C1s spectra (Fig. 9a). This is likely due to the formation of SEI layer as a consequence of the electrolyte decomposition on the surface of the material as confirmed by the presence of two intense peaks in the C1s spectra. These peaks placed at 285.9 eV and around 291−292 eV corresponds to CH_x-groups in polyethylene oxide polymer (CH_2-CH_2-O, PEO) formed by polymerization of EC and to Li carbonate (Li alkylcarbonates, $ROCO_2Li$ (LACs) and/or Li_2CO_3) species, which originated from the reductive decomposition of EC, PC, and DMC, respectively [3,37].

Ar ion etching was further performed at different times up to 360 min to obtained information about the SEI composition and lithiation compounds. The evolution of the C1s spectra shows progressive decrease of the SEI products with the etching time. Firstly, the CH_x-compounds are removed after only 0.5 min of etching, while the carbonate species are almost completely vanished after 20 min of etching. This suggests a higher amount of carbonate species in the SEI composition compared to polyethylene oxide. These carbonates are of crystalline nature since were also detected by XRD (Fig. 8a).

Once the CH_x species disappeared, we can observe the appearance of the Csp^2 peak (284.5 eV) at 5 min of etching which gradually increases with the etching time and becomes the unique component at 20 min of etching. The Si species are observed as well after 20 min of etching, therefore after the removal of SEI layer (Fig. 9b) and a typical Si2p spectra is characterized by one peak, which was deconvoluted into 2 contributions, i.e., $Si2p_{3/2}$ and $Si2p_{1/2}$ placed at 102.1 and 102.7 eV. The position of these peaks is different compared to the material before cycling, i.e., placed at 103.8 eV and corresponding to SiO_2 species. This indicates the formation of different species which can be assigned according to the literature to Si−O−Li in Li silicates (Li_xSiO_y), most likely Li_4SiO_4. When increasing the etching time, the Si2p position slightly shifts to lower binder energies, i.e., 101.7 eV and 102.3 eV, therefore the presence of other lithium silicate phases such as $Li_2Si_2O_5$ cannot either be excluded [36]. However, no Si (99.5 eV) or Li_xSi alloy (96.0−97.3 eV) [37,38] was observed even after 360 min of etching, the peak position remaining rather in the same place. Similar results were reported by Guo et al. by using NMR technique [35].

Contribution of Li and F has been also detected on the initial material and after etching as illustrated in Fig. S6, SI. Li1s peak is placed to 55.6 eV and corresponds to Li_2O and LiF. The presence lithium fluoride (LiF) is also confirmed by the position of F1s peak placed at ~685 eV and is one of the main degradation products of $LiPF_6$ electrolyte salt [39].

These results suggest that the first layer of SEI is composed by LACs and ethylene oxides, the later one being removed after 0.5 min of etching. Between 0.5 and 5 min concomitant removal of LACs species with the appearance of sp^2 carbon and Li_2O/Li_4SiO_4 species

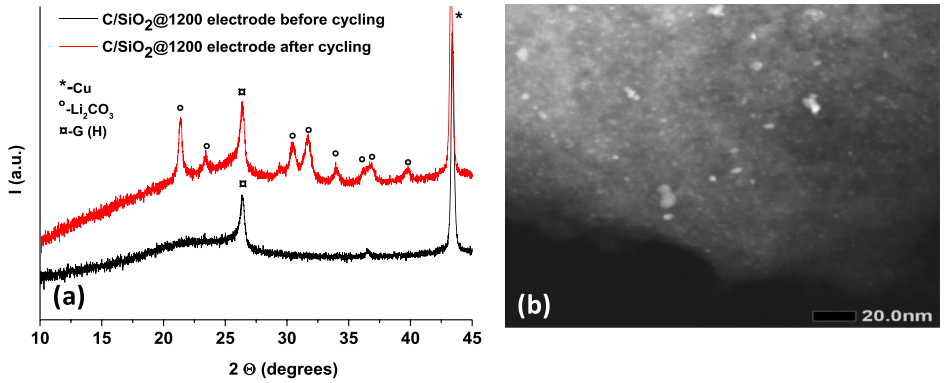

Fig. 8. XRD analysis before and after 250 cycles for C/SiO_2@900 electrode recovered after discharge step (a), STEM images after cycling for C/SiO_2@900 (b). (A colour version of this figure can be viewed online.)

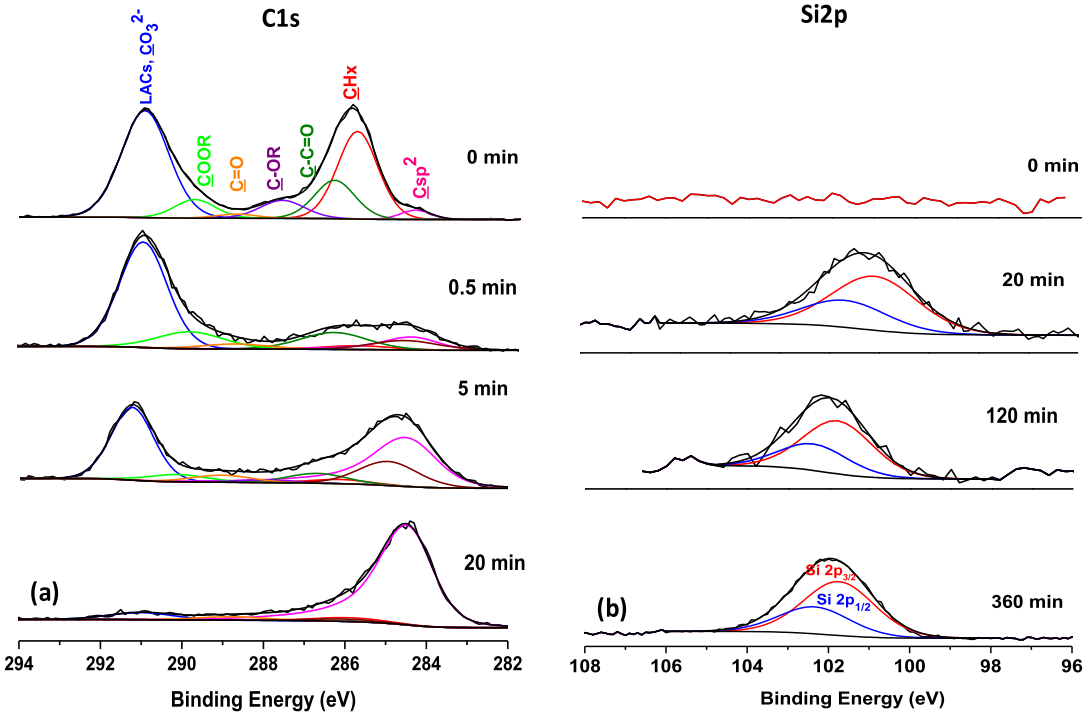

Fig. 9. XPS high resolution spectra of C1s (a) and Si2p (b) at various Ar etching times for C/SiO_2@900 material after cycling. (A colour version of this figure can be viewed online.)

occurs. Therefore, at 5 min of etching, the C/Si based material start to be observed and is more present as the etching time increases to 20 min in the detriment of SEI which disappears. For longer etching times (>20 min and up to 360 min), lithium silicate species are detected.

Based on the analyses performed herein, we will try to suggest a mechanism of lithiation of confined nano-sized SiO_2 particles in hard carbon. The lithiation mechanism of SiO_2 is not yet well understood and the compounds formed due to the conversion reaction of SiO_2 still controversial. For many years, the SiO_2 was considered an inert phase to lithiation owing to the strong Si–O bond which is not able to be cleaved by the insertion of Li. The main electrochemical reactions reported in the literature for the lithiation of SiO_2 (Eqs. (1)–(3)) [4,6,34,35] are based on the formation of Li_2O and lithium silicate compounds (Li_4SiO_4) along with Si (Eqs. (1) and (2)). The formation of Li_2O and Li_4SiO_4 is irreversible, these compounds cannot be delithiated and then contribute, besides carbon, to the high irreversible capacity loss during the first charge/discharge cycles. They are considered to be inactive for subsequent cycling, but they can likely accommodate the volume change and prevent the particle agglomeration during lithiation/delithiation [5,13]. The Li is inserted in the newly electrochemically formed Si (Eqs. (1) and (2)) resulting in Si alloys, i.e., $Li_{15}Si_4$. This reaction is reversible according to Eq. (3):

$$4\,Li^+ + 4e^- + SiO_2 \rightarrow 2Li_2O + Si \quad (1)$$

$$4\,Li^+ + 4e^- + 2SiO_2 \rightarrow Li_4SiO_4 + Si \quad (2)$$

$$Si + xLi^+ + xe^- \leftrightarrow Li_xSi \quad (3)$$

Our results did not reveal the presence of Si or Li_xSi phases either by XRD or XPS under Ar etching. In addition, the electrochemical derivative curves did not evidence peaks corresponding

to the formation of Li_xSi around 0.25−0.32 V [20,34]. However, the absence of such peaks may be related, in some cases, to the small size of SiO_2 [40] and slow kinetics related to their confinement in the carbon matrix. The observed gradual increase of the specific capacity during cycling was explained in the literature by the reduction of SiO_2 with the formation of Si which is able to insert more and more Li [4,19,20,41]. However, the mechanism behind is not well demonstrated.

Recent works pointed out by using different experimental analyses techniques another type of lithiation mechanisms for SiO_2 *via* a reversible insertion of Li into SiO_2 structure [36,42] with the formation of other lithium silicate phases ($Li_2Si_2O_5$, Li_2SiO_3) according to Eqs. (4) and (5), in addition to the formation silicon alloys, Li_xSi (Eq (3)).

$$4\,Li^+ + 4e^- + 5SiO_2 \leftrightarrow 2Li_2Si_2O_5 + Si \quad (4)$$

$$4\,Li^+ + 4e^- + 3SiO_2 \leftrightarrow 2Li_2SiO_3 + Si \quad (5)$$

Theoretical studies demonstrated as well that the $Li_2Si_2O_5$ phase has the highest probability to be formed by insertion of Li into SiO_2 and that this process was found to be very exothermic [34]. The electrochemical potential of the formation of this phase is expected around 0.22−0.77 V according to different works summarized by Lener G. et al. [34]. In our case we observed as well a large peak ~0.2−0.4 V which may correspond to $Li_2Si_2O_5$ and XPS analyses confirmed also the presence of lithium silicate species. Therefore, the mechanism of lithiation of our nano-SiO_2 confined in hard carbon is likely to occur via the irreversible reactions (Eqs. (1) and (2)) and the reversible reactions (Eqs. (4) and (5)), no evidence of silicon alloys being observed contrary to previous works.

4. Conclusions

A novel eco-friendly, simple and fast one-pot synthesis route to prepare hard carbon/SiO_2 materials was developed. This way of preparation allows successfully obtaining hybrid materials containing SiO_2 amorphous nanoparticles (2−5 nm) homogenously dispersed in the carbon framework. By increasing the synthesis temperature from 600 to 1200 °C, the textural properties (surface area/pore volume) and the amount of oxygen functional groups were significantly decreased resulting in a decrease of the irreversible capacity loss during the first cycles. The increase of the annealing temperature (from 600 °C to 1200 °C) has also a positive impact on the reversible capacity, which raised from 224 mA hg^{-1} to 535 mA hg^{-1}. However, an atypical electrochemical behavior was observed between the 2nd and 50th cycle, i.e., increase of the capacity with the number of cycles which was more pronounced with the increase of the annealing temperature. This could be related to the decrease of the hydrophilic behavior and of the porosity of the materials as well as to the confinement of the SiO_2 nanoparticles in the carbon network limiting therefore the electrolyte diffusion and the electrochemical reaction occurrence. Once this "activation" process initiated, a stable capacity higher than 500 mA hg^{-1} could be maintained for more than 250 cycles. This excellent cycle stability was correlated to the SiO_2 confinement in the carbon network which buffer the volume expansion and maintain small and dispersed particles. XRD and XPS post-mortem analyses suggested a SiO_2 lithiation mechanism pathway different than most of the reported works which occurs *via* the reversible formation of lithium silicates.

Acknowledgements

The authors gratefully acknowledge the financial support of this work from Université de Haute-Alsace, France through the Ph. D scholarship of Cristina Nita. We thank Loïc Vidal for performing the STEM analyses *via* the IS2M-Mulhouse technical platforms.

Appendix A. Supplementary data

Supplementary data to this article can be found online at https://doi.org/10.1016/j.carbon.2018.11.069.

References

[1] J.-M. Tarascon, M. Armand, Issues and challenges facing rechargeable lithium batteries, Nature 414 (2001) 359−367.
[2] E. Peled, C. Menachem, D. Bar-Tow, A. Melman, Improved graphite anode for lithium-ion batteries. chemically bonded solid electrolyte interface and nanochannel formation, J. Electrochem. Soc. 143 (1996) L4−L7.
[3] C. Matei-Ghimbeu, C. Decaux, P. Brender, M. Dahbl, D. Lemordant, E. Raymundo-Piñero, et al., Influence of graphite characteristics on the electrochemical performance in alkylcarbonate LiTFSI electrolyte for Li-ion capacitors and Li-ion batteries, J. Electrochem. Soc. 160 (2013) A1907−A1915.
[4] Z. Favor, W. Wang, H. Bay, A. George, M. Ozkan, S. Ozkan, Stable cycling of SiO_2 nanotubes as high-performance anodes for lithium-ion batteries, Sci. Rep. 4 (2014), 04605.
[5] N. Yan, F. Wang, H. Zhong, Y. Li, Y. Wang, L. Hu, et al., Hollow porous SiO_2 nanocubes towards high-performance anodes for lithium-ion batteries, Sci. Rep. 3 (2013) 1568.
[6] K. Kim, J.-H. Park, S.-G. Doo, T. Kim, Effect of oxidation on Li-ion secondary battery with non-stoichiometric silicon oxide (SiO_x) nanoparticles generated in cold plasma, Thin Solid Films 518 (2010) 6547−6549.
[7] J.-Y. Lim, D. Nguyen, J.-S. Kang, S.-W. Song, Facile synthesis and stable cycling ability of hollow submicron silicon oxide-carbon composite anode material for Li-ion battery, J. Alloy. Comp. 633 (2015) 92−96.
[8] L. Li, P. Liu, K. Zhu, J. Wang, G. Tai, J. Liu, Flexible and robust N-doped carbon nanofiber film encapsulating uniformly silica nanoparticles: free-standing long-life and low-cost electrodes for Li- and Na-Ion batteries, Electrochem Acta 235 (2017) 79−87.
[9] M. Obrovac, L. Christensen, Structural changes in silicon anodes during lithium insertion/extraction, Electrochem. Solid State Lett. 7 (2004) A93−A96.
[10] H. Wu, Y. Cui, Designing nanostructured Si anodes for high energy lithium ion batteries, Nano Today 7 (2012) 414−429.
[11] A. Casimir, H. Zhang, O. Ogoke, J. Amine, J. Lu, G. Wu, Silicon-based anodes for lithium-ion batteries: effectiveness of materials synthesis and electrode preparation, Nanomater. Energy 27 (2016) 359−376.
[12] Z.-L. Xu, X. Liu, Y. Luo, L. Zhou, J.-K. Kim, Nanosilicon anodes for high performance rechargeable batteries, Prog. Mater. Sci. 90 (2017) 1−44.
[13] J. Wang, H. Zhao, J. He, C. Wang, J. Wang, Nano-sized SiO_x/C composite anode for lithium ion batteries, J. Power Sources 196 (2011) 4811−4815.
[14] J. Tang, A. Dysart, D. Kim, R. Saraswat, G. Shaver, V. Pol, Fabrication of carbon/silicon composite as lithium-ion anode with enhanced cycling stability, Electrochem Acta 247 (2017) 626−633.
[15] Z. Li, Z. Li, W. Zhong, C. Li, L. Li, H. Zhang, Facile synthesis of ultrasmall Si particles embedded in carbon framework using Si-carbon integration strategy with superior lithium ion storage performance, Chem. Eng. J. 319 (2017) 1−8.
[16] J. Wang, H. Ren, Y. Chen, K. Zhang, O. Ken, W. Zhang, et al., Synthesis of high-quality mesoporous silicon particles for enhanced lithium storage performance, Mater. Chem. Phys. 173 (2016) 89−94.
[17] D. Nguyen, C. Nguyen, J.-S. Kim, J.-Y. Kim, S.-W. Song, Facile synthesis and high anode performance of carbon fiber-interwoven amorphous nano-SiO_x/graphene for rechargeable lithium batteries, ACS Appl. Mater. Interfaces 5 (2013) 11234−11239.
[18] A. Cadiz Bedini, B. Klingebiel, M. Luysberg, R. Carius, Sonochemical synthesis of hydrogenated amorphous silicon nanoparticles from liquid trisilane at ambient temperature and pressure, Ultrason. Sonochem. 39 (2017) 883−888.
[19] H. Xia, Z. Yin, F. Zheng, Y. Zhang, Facile synthesis of SiO_2/C composites as anode materials for lithium-ion batteries, Mater. Lett. 205 (2017) 83−86.
[20] S. Hao, Z. Wang, L. Chen, Amorphous SiO_2 in tunnel-structured mesoporous carbon and its anode performance in Li-ion batteries, Mater. Des. 111 (2016) 616−621.
[21] X. Liu, Y. Chen, H. Liu, Z.-Q. Liu, SiO2@C hollow sphere anodes for lithium-ion batteries, J. Mater. Sci. Technol. 33 (2017) 239−245.
[22] Y.-K. Kim, J.-W. Moon, J.-G. Lee, Y.-K. Baek, S.-H. Hong, Porous carbon-coated silica macroparticles as anode materials for lithium ion batteries: effect of boric acid, J. Power Sources 272 (2014) 689−695.
[23] X. Zhang, Q. Yan, W. Leng, J. Li, J. Zhang, Z. Cai, et al., Carbon nanostructure of kraft lignin thermally treated at 500 to 1000 C, Materials 10 (2017) 975.
[24] C. Pardanaud, C. Martin, G. Giacometti, N. Mellet, B. Pégourié, P. Roubin, Thermal stability and long term hydrogen/deuterium release from soft to hard amorphous carbon layers analyzed using in-situ Raman spectroscopy. Comparison with Tore Supra deposits, Thin Solid Films 581 (2015) 92−98.
[25] J.-T. Jiu, H. Wang, C.-B. Cao, H.-S. Zhu, The effect of annealing temperature on the structure of diamond-like carbon films by electrodeposition technique,

J. Mater. Sci. 34 (1999) 5205–5209.
[26] A. Maetz, L. Delmotte, G. Moussa, J. Dentzer, S. Knopf, C. Matei-Ghimbeu, Facile and sustainable synthesis of nitrogen-doped polymer and carbon porous spheres, Green Chem. 19 (2017) 2266–2274.
[27] E. Buiel, A. George, J. Dahn, Model of micropore closure in hard carbon prepared from sucrose, Carbon 37 (1999) 1399–1407.
[28] C. Matei Ghimbeu, J. Górka, V. Simone, L. Simonin, S. Martinet, C. Vix-Guterl, Insights on the Na^+ ion storage mechanism: discrimination between the hard carbon porosity, surface chemistry and active surface area, Nanomater. Energy 44 (2018) 327–335.
[29] A. Beda, P.-L. Taberna, P. Simon, C. Matei Ghimbeu, Hard carbons derived from green phenolic resins for Na-ion batteries, Carbon 139 (2018) 248–257.
[30] C. Matei Ghimbeu, M. Sopronyi, F. Sima, J. Le Meins, C. Vaulot, C. Zlotea, et al., One-pot laser-assisted synthesis of porous carbons with embedded magnetic cobalt particles, Nanoscale 7 (22) (2015) 10111–10122.
[31] C. Nita, M. Bensafia, C. Vaulot, L. Delmotte, C. Matei Ghimbeu, Insights on the synthesis mechanism of green phenolic resin derived porous carbons via a salt-soft templating approach, Carbon 109 (2016) 227–238.
[32] L. Chen, K. Wang, X. Xie, J. Xie, Effect of vinylene carbonate (VC) as electrolyte additive on electrochemical performance of Si film anode for lithium ion batteries, J. Power Sources 174 (2007) 538–543.
[33] N.-S. Choi, S.-Y. Ha, Y. Lee, J. Jang, M.-H. Jeong, W. Shin, et al., Recent progress on polymeric binders for silicon anodes in lithium-ion batteries, J Electrochem Sci Tech 6 (2015) 35–49.
[34] G. Lener, M. Otero, D. Barraco, E. Leiva, Energetics of silica lithiation and its applications to lithium ion batteries, Electrochem Acta 259 (2018) 1053–1058.
[35] B. Guo, J. Shu, Z. Wanga, H. Yang, L. Shi, L. Chen, Electrochemical reduction of nano-SiO2 in hard carbon as anode material for lithium ion batteries, Electrochem. Commun. 10 (2008) 1876–1878.
[36] Q. Sun, B. Zhang, W.-Z. Fu, Lithium electrochemistry of SiO2 thin film electrode for lithium-ion batteries, Appl. Surf. Sci. 254 (2008) 3774–3779.
[37] H. Takezawa, S. Ito, H. Yoshizawa, T. Abe, Surface composition of a SiOx film anode cycled in carbonate electrolyte for Li-ion batteries, Electrochim. Acta 229 (2017) 438–444.
[38] B. Philippe, R. Dedryvère, J. Allouche, F. Lindgren, M. Groi, H. Rensmo, et al., Nanosilicon electrodes for lithium-ion batteries: interfacial mechanisms studied by hard and soft X-ray photoelectron spectroscopy, Chem. Mater. 24 (2012) 1107–1115.
[39] M. Nie, D. Abraham, D. Seo, Y. Chen, A. Bose, B. Lucht, Role of solution structure in solid electrolyte interphase formation on graphite with $LiPF_6$ in propylene carbonate, J. Phys. Chem. C 117 (2013) 25381–25389.
[40] F. Lepoivre, D. Larcher, J.-M. Tarascon, Electrochemical activation of silica for enhanced performances of Si-based electrodes, J. Electrochem. Soc. 163 (2016) A2791–A2796.
[41] C. Ban, B. Kappes, Q. Xu, C. Engtrakul, C. Ciobanu, A. Dillon, et al., Lithiation of silica through partial reduction, Appl. Phys. Lett. 100 (2012), 243905-1-4.
[42] W.-S. Chang, C.-M. Park, J.-H. Kim, Y.-U. Kim, G. Jeong, H.-J. Sohn, Quartz (SiO_2): a new energy storage anode material for Li-ion batteries, Energy Environ. Sci. 5 (2012) 6895–6899.